applied sciences

MDPI

Article

Based on Backpropagation Neural Network and Adaptive Linear Active Disturbance Rejection Control for Attitude of a Quadrotor Carrying a Load

Yunlong Gao, Guixin Zhu * and Tong Zhao

College of Automation and Electronic Engineering, Qingdao University of Science and Technology, Qingdao 266061, China
* Correspondence: qdzgxqust@163.com; Tel.: +86-186-6980-5259

Abstract: A control method combining Backpropagation (BP) neural network and Adaptive Linear Active Disturbance Rejection Control (ALADRC) is proposed for the attitude control problem of quadrotor aircraft. The proposed controller can observe and compensate the total disturbance in the working process of the quadrotor system. At the same time, it has a good ability to suppress the disturbance of the quadrotor load mass change. In addition, adaptive control and BP neural network are used to adjust the controller parameters in real time to solve the problem of difficult parameter tuning. Finally, the stability of the system is proved based on Lyapunov theory. The simulation results show that the quadrotor system can still track the altitude and attitude angle commands stably in the presence of disturbances, and has strong adaptability to load mass changes, so that the quadrotor can still complete the given tasks in the presence of multi-source disturbances.

Keywords: Backpropagation neural network; attitude control; total disturbance; adaptive control; parameter tuning

Citation: Gao, Y.; Zhu, G.; Zhao, T. Based on Backpropagation Neural Network and Adaptive Linear Active Disturbance Rejection Control for Attitude of a Quadrotor Carrying a Load. *Appl. Sci.* **2022**, *12*, 12698. https://doi.org/10.3390/app122412698

Academic Editor: Emanuele Carpanzano

Received: 19 November 2022
Accepted: 9 December 2022
Published: 11 December 2022

1. Introduction

Today, quadrotors have become popular in many application scenarios due to their high flexibility and high degrees of freedom, such as power inspection, data collection, surveillance and reconnaissance missions, forest fire rescue, and precision agriculture [1–3].

The quadrotor system is a typical underactuated system, which has the characteristics of nonlinearity, strong coupling, and susceptibility to interference, so it is difficult to establish an accurate mathematical model. A way to design a controller with high stability and strong robustness is a difficult research point. Due to the advantages of simple structure and easy implementation, linear controllers are widely used in quadrotor control systems. Research by Shakeel et al. [4] presented that the Linear Quadratic Regulator (LQR) controller has a good control effect by analyzing and evaluating several different control schemes of the quadrotor. However, many scholars still try to use modern control methods to improve the control performance of quadrotor controllers, such as predictive control [5,6], sliding film control [7], LQR [8,9] and so on. Based on backstepping control and Lyapunov theory, research by Rodríguez et al. [10] presented a robust control algorithm in order to increase the endurance time of the quadrotor and reduce unnecessary energy dissipation. Research by Nigro et al. [11] presented a new type of quadrotor aircraft by adding a driving gimbal mechanism to provide multi-directional thrust. At the same time, a double closed-loop motion control scheme was proposed to enhance the robustness of the system. However, the above studies are all based on the nominal conditions of the quadrotor, that is, the influence of disturbance is ignored. This leads to the poor control effect of the controller designed in some scenes with large disturbances.

The quadrotors are usually affected by external unknown wind disturbances and unmodeled dynamics within the system, which will lead to poor stability of the quadrotor

system. Designing a robust controller to overcome the influence of disturbances to ensure the stability of the quadrotor system has always been a key topic for some scholars. For example, considering the uncertainty of system parameters, research by Fan et al. [12] presented a control scheme combining neural network and adaptive control, and provided the simulation results. Based on the backstepping control theory, research by Chen et al. [13] presented a nonlinear adaptive integral backstepping control algorithm. The simulation results prove that the controller still has strong robustness in the presence of wind disturbance. However, these studies did not address specific mathematical models of wind disturbance, nor did they explain how wind disturbance acts on the system.

Nowadays, in order to solve the problem of unknown disturbance of the quadrotor system, many scholars have carried out in-depth research on the quadrotor control system based on the Active Disturbance Rejection Control (ADRC) theory. The ADRC does not require an accurate mathematical model of the controlled object, and its structure is simple, so it can be used in the controller design of a quadrotor system [14]. Aiming at the problem that the ADRC controller has many parameters, it is difficult to tune these parameters. Research by Zhang et al. [15] applied the fractional fuzzy particle swarm optimization (FOFPSO) algorithm to optimize the ADRC controller parameters, and it was compared with several other optimization algorithms to optimize the ADRC parameters. Finally, the authors propose a novel wind field model; this model is employed to prove the effectiveness of the controller under the action of wind disturbance. Research by Yuan and Zhao et al. [16,17], aiming at the problem of grid voltage fluctuation in power grid systems such as wind power grid-connected inverters, proposed an improved LADRC controller to improve the disturbance observation accuracy of the system by reducing the phase lag of the observer. The results showed that the improved method has better rapidity and immunity.

Linear Active Disturbance Rejection (LADRC) is widely used because of the small number of controller parameters and convenient adjustment [18–21]. Although the number of controller parameters that need to be adjusted by LADRC is much smaller than that of ADRC, it is still a difficult task to readjust the controller parameters for different systems or the same system in different working scenarios. At the same time, Linear Extension State Observer (LESO) in LADRC often has the problem of limited bandwidth, which may cause poor control effect in practical applications [22].

For the problem of quadrotor attitude control, this paper designs a quadrotor attitude control strategy based on LADRC. The control strategy not only considers the internal and external disturbances of the system, but also has a strong adaptability to load quality changes. In order to solve the problem of LADRC controller having too many parameters and being difficult to adjust manually, BP neural network and adaptive control algorithm are proposed in this paper. The BP neural network is used to dynamically optimize and adjust the bandwidth value of LESO in real time, so that the controller can still maintain good control effect in the complex and changeable working environment. By adjusting the values of k_p and k_d in the PD controller in real time, adaptive control reduces the parameter error caused by manual parameter adjustment, and compensates the observation error caused by bandwidth selection, which improves the control accuracy of LADRC and the dynamic performance of the system. Finally, in order to verify the effectiveness of the control scheme, a simulation experiment is designed to verify the attitude tracking ability of the controller.

2. Dynamic Model of Quadrotor Aircrafts

The coordinate system and structure of the quadrotor are shown in Figure 1. We use six variables to describe the motion of the quadrotor, namely the quadrotor position x, y, z, the attitude angle ϕ, θ and ψ [23]. The centroid of quadrotor moves upward continuously from below the origin of the fuselage mount when the load is gradually reduced. Referring to the body coordinate system B and the ground fixed coordinate system E, the dynamic model of the variable mass quadrotor aircraft is established [24].

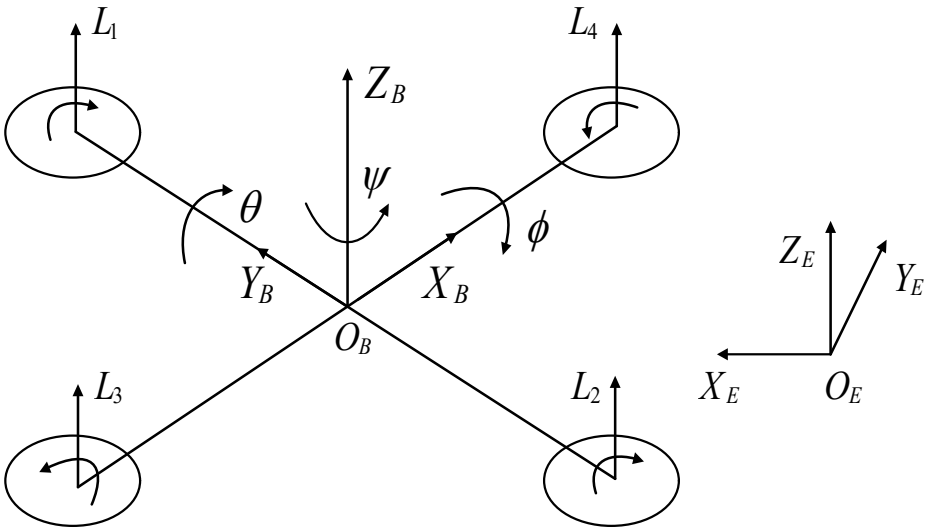

Figure 1. Structure diagram of a quadrotor.

As shown in Figure 1, the rotation matrix from coordinate system B to E is $R_{B\to E}$ [25,26]. The positional motion of the quadrotor satisfies Newton's second law,

$$\begin{cases} \dot{X}^E = V^E \\ (M-\Delta m)\dot{V}^E = L^E + G_M^E + G_{\Delta m}^E + f_1^E \end{cases}, \tag{1}$$

where $X^E = [x \quad y \quad z]^T$; V^E is the linear velocity; M is the mass of the quadrotor; L^E is the total lift; $G_{\Delta m}^E = [0 \quad 0 \quad \Delta mg]^T$; $G_M^E = [0 \quad 0 \quad -Mg]^T$; $f_1^E = [-k\dot{x} \quad -k\dot{y} \quad -k\dot{z}]^T$ is the matrix of air resistance.

The lift force of the quadrotor is expressed as

$$L^B = [L_x \quad L_y \quad L_z]^T = [0 \quad 0 \quad L]^T, \tag{2}$$

where $L = \sum_{i=1}^{4} L_i = L_1 + L_2 + L_3 + L_4$; from $R_{B\to E}$, we can obtain L^E:

$$L^E = R_{B\to E} L^B = L \begin{bmatrix} \sin\psi\sin\phi + \cos\phi\cos\psi\sin\theta \\ -\sin\phi\cos\psi + \cos\phi\sin\psi\sin\theta \\ \cos\phi\cos\theta \end{bmatrix}. \tag{3}$$

In summary, we can obtain the positional dynamics equation of the quadrotor.

$$\begin{cases} \ddot{x} = \frac{-k_f\dot{x}}{(M-\Delta m)} + \frac{L(\sin\psi\sin\phi + \cos\psi\cos\phi\sin\theta)}{(M-\Delta m)} \\ \ddot{y} = \frac{-k_f\dot{y}}{(M-\Delta m)} + \frac{L(-\cos\psi\sin\phi + \sin\psi\cos\phi\sin\theta)}{(M-\Delta m)} \\ \ddot{z} = \frac{-k_f\dot{z}}{(M-\Delta m)} + \frac{L\cos\phi\cos\theta}{(M-\Delta m)} - g \end{cases}. \tag{4}$$

As the load mass decreases, the centroid of quadrotor gradually moves upward, thereby affecting the attitude angle of the quadrotor. Because the quadrotor is loaded by the mounting platform, the two can be considered as a whole. The initial coordinates of the centroid of quadrotor are (x_1, y_1, z_1), the coordinates of the centroid of the part of the load

that is reduced during operation are (x_2, y_2, z_2). When the load mass decreases, the change in the coordinates of the centroid of quadrotor is shown in the following formula:

$$\begin{cases} x_a = (x_1 M - x_2 \Delta m)/(M - \Delta m) \\ y_a = (y_1 M - y_2 \Delta m)/(M - \Delta m) \\ z_a = (z_1 M - z_2 \Delta m)/(M - \Delta m) \end{cases}, \tag{5}$$

where the coordinates of the centroid of the quadrotor are (x_a, y_a, z_a). According to Figure 1, initial coordinate of the centroid of the quadrotor is $(0, 0, 0)$, the coordinate of the centroid of the reduced load mass during the working process is $(0, 0, z_c)$. Substituting it into Formula (6), the coordinate of the centroid of the quadrotor can be obtained as $(0, 0, z_a)$.

$$z_a = z_c m/(M - \Delta m). \tag{6}$$

According to the Newton–Euler equation, the attitude dynamics equation can be expressed as [27].

The attitude angle motion of the quadrotor satisfies the Newton–Euler equation, and its attitude dynamic model can be expressed as [28,29]

$$\begin{cases} I_{3\times3}\dot{\tau}^B + \tau^B \times I_{3\times3}\tau^B = \varsigma^B \\ \varsigma^B = Q^B + f_2^B + P^B \end{cases}, \tag{7}$$

where $I_{3\times3} = diag(I_x, I_y, I_z)$ is the inertia matrix; $\tau^B = [\dot{\phi} \quad \dot{\theta} \quad \dot{\psi}]^T$ is the angular velocity; ς^B is the resultant moment; P^B and Q^B are the pulling torque and reaction torque of the four-wheel drive motor, respectively; $f_2^B = [-lk_f\dot{\phi} \quad -lk_f\dot{\theta} \quad -k_f\dot{\psi}]^T$ is the matrix of air resistance.

$$P^B = \begin{bmatrix} b_1\sqrt{l^2 - z_a^2}(-L_1 + L_2 + L_3 - L_4) \\ b_1\sqrt{l^2 - z_a^2}(-L_1 - L_2 + L_3 + L_4) \\ 0 \end{bmatrix}, \tag{8}$$

$$Q^B = \begin{bmatrix} 0 \\ 0 \\ b_2(L_1 - L_2 + L_3 - L_4) \end{bmatrix}. \tag{9}$$

In summary, we can obtain attitude dynamics equation of the quadrotor.

$$\begin{cases} \ddot{\phi} = -lk_f\dot{\phi}/I_x + b_1\sqrt{l^2 - z_a^2}(-L_1 + L_2 + L_3 - L_4)/I_x + (I_y - I_z)\dot{\psi}\dot{\theta}/I_x \\ \ddot{\psi} = -k_f\dot{\psi}/I_z + b_2(L_1 - L_2 + L_3 - L_4)/I_z + (I_x - I_y)\dot{\phi}\dot{\theta}/I_z \\ \ddot{\theta} = -lk_f\dot{\theta}/I_y + b_1\sqrt{l^2 - z_a^2}(-L_1 - L_2 + L_3 + L_4)/I_y + (I_z - I_x)\dot{\phi}\dot{\psi}/I_y \end{cases}, \tag{10}$$

where ψ, ϕ, and θ are the yaw angle, roll angle and pitch angle, respectively.

To simplify the quadrotor dynamic equation, (U_1,U_2,U_3,U_4) is used to represent the relevant parameters.

$$\begin{bmatrix} U_1 \\ U_2 \\ U_3 \\ U_4 \end{bmatrix} = \begin{bmatrix} \frac{1}{(M-\Delta M)} & \frac{1}{(M-\Delta M)} & \frac{1}{(M-\Delta M)} & \frac{1}{(M-\Delta M)} \\ -\frac{b_1}{I_x} & \frac{b_1}{I_x} & \frac{b_1}{I_x} & -\frac{b_1}{I_x} \\ -\frac{b_1}{I_y} & -\frac{b_1}{I_y} & \frac{b_1}{I_y} & \frac{b_1}{I_y} \\ \frac{b_2}{I_z} & -\frac{b_2}{I_z} & \frac{b_2}{I_z} & -\frac{b_2}{I_z} \end{bmatrix} \begin{bmatrix} L_1 \\ L_2 \\ L_3 \\ L_4 \end{bmatrix}. \tag{11}$$

In summary, we can obtain the dynamic equation of the quadrotor.

$$\begin{cases} \ddot{x} = -k_f\dot{x}/(M-\Delta m) + U_1(\sin\phi\sin\psi + \cos\psi\cos\phi\sin\theta) \\ \ddot{y} = -k_f\dot{y}/(M-\Delta m) + U_1(-\sin\phi\cos\psi + \sin\psi\cos\phi\sin\theta) \\ \ddot{z} = -k_f\dot{z}/(M-\Delta m) - g + U_1\cos\phi\cos\theta \\ \ddot{\theta} = U_3\sqrt{l^2-z_a^2} + (I_z-I_x)\dot{\phi}\dot{\psi}/I_y - lk_f\dot{\theta}/I_y \\ \ddot{\phi} = U_2\sqrt{l^2-z_a^2} + (I_y-I_z)\dot{\theta}\dot{\psi}/I_x - lk_f\dot{\phi}/I_x \\ \ddot{\psi} = U_4 + (I_x-I_y)\dot{\phi}\dot{\theta}/I_z - k_f\dot{\psi}/I_z \end{cases}. \tag{12}$$

Equation (13) can also be written as [30]

$$\begin{cases} \dot{x}_1 = x_2 \\ \dot{x}_2 = Au(n) + B + c \end{cases}', \tag{13}$$

where $x_1 = \begin{bmatrix} z & \phi & \theta & \psi \end{bmatrix}^T$, $u(n) = \begin{bmatrix} U_1 & U_2 & U_3 & U_4 \end{bmatrix}^T$;

$$A = \begin{bmatrix} \cos\theta\cos\phi & 0 & 0 & 0 \\ 0 & \sqrt{l^2-z_a^2} & 0 & 0 \\ 0 & 0 & \sqrt{l^2-z_a^2} & 0 \\ 0 & 0 & 0 & 1 \end{bmatrix} B = \begin{bmatrix} -g - k_f\dot{z}/(M-\Delta M) \\ -lk_f\dot{\phi}/I_x + (I_y-I_z)\dot{\psi}\dot{\theta}/I_x \\ -lk_f\dot{\theta}/I_y + (I_z-I_x)\dot{\psi}\dot{\phi}/I_y \\ -k_f\dot{\psi}/I_z + (I_x-I_y)\dot{\phi}\dot{\theta}/I_z \end{bmatrix}.$$

3. Control Scheme Design

Aiming at the problems of strong coupling, nonlinearity and mass change of the quadrotor system, we proposed a control scheme combining BP neural network, adaptive controller and LADRC. The BP-ALDRC control system of quadrotor under the condition of continuous time-varying wind field disturbance and changing load quality is established. Figure 2 is a block diagram of the control scheme.

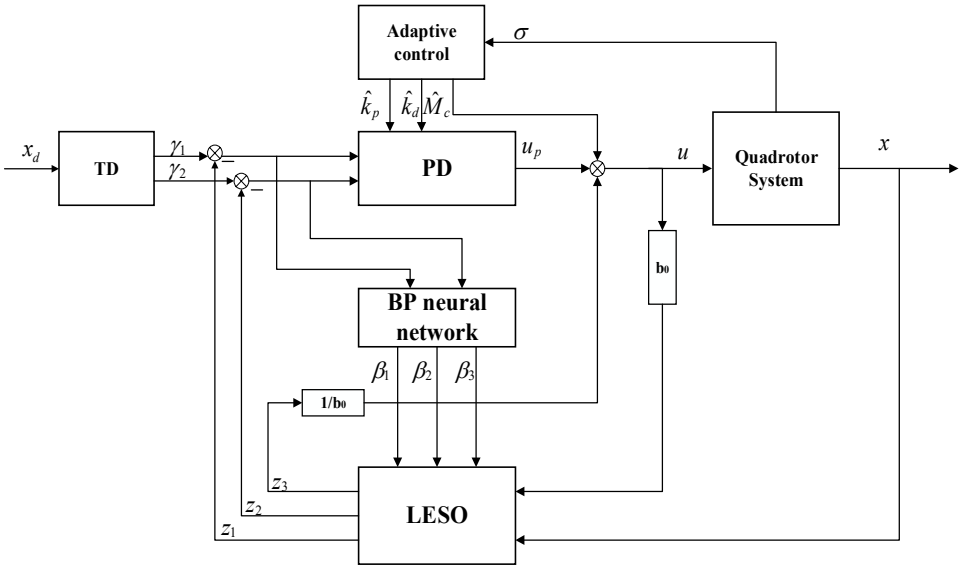

Figure 2. Control scheme structure diagram.

In this Figure, x_d is the given signal, $\begin{bmatrix} z_1 & z_2 & z_3 \end{bmatrix}$ is the observation vector of LESO to the system state variable, $\begin{bmatrix} \beta_1 & \beta_2 & \beta_3 \end{bmatrix}$ is the bandwidth gain vector of LESO, $\begin{bmatrix} \gamma_1 & \gamma_2 \end{bmatrix}$ is the approximate value of the given signal and its differential, u_p is a nonlinear state error feedback control law with PD controller output, u is the control law of the system, σ is the error combination, $\hat{k}_p, \hat{k}_d$ are the estimated values of PD controller parameters k_p, k_d,

respectively, $\hat{M}_c$ is the estimated value of load mass change M_c, x is the state variable of the system, b_0 is the compensation factor.

The advantage of using LADRC to control the quadrotor is that there is no need to decouple the channels. LADRC directly estimates system internal disturbances such as system coupling and environmental external disturbances in the working process as the total disturbance for observation and compensation. Aiming at the difficulty of setting LADRC parameters and avoiding errors caused by manual parameter adjustment, we use adaptive control to adjust the PD controller parameters in real time.

4. Control Methodology

4.1. Design of LADRC Controller

The dynamic Equation (12) can be transformed into

$$\begin{cases} \dot{\vartheta}_1 = \vartheta_2 \\ \dot{\vartheta}_2 = q(t) + d(t) + Gu(x) \\ y = \vartheta_1 \end{cases}, \tag{14}$$

where $\vartheta = [\vartheta_1 \ \vartheta_2]^T$ are measurable state variables; y is the output signal; $f(t)$ is an unknown nonlinear function of the system; $d(t)$ is the external disturbance. G a is partially known, and the known part is denoted as G_0.

All uncertainties in the system and all disturbances received by the system are regarded as the total disturbance, which is defined as

$$F(\vartheta, u(\vartheta)) = f(t) + [g(t) - b_0]u(\vartheta) + d(t). \tag{15}$$

To observe the total disturbance, the extended state space is defined $\zeta = [\zeta_1 \ \zeta_2 \ \zeta_3]$, where $\zeta_1 = \vartheta_1$, $\zeta_2 = \dot{\vartheta}_1$ and $\zeta_3 = F(\vartheta, u(\vartheta))$.

The nonlinear system (12) can be transformed into

$$\begin{cases} \dot{\zeta} = M\zeta + Nu + Th \\ y = U\zeta \end{cases}, \tag{16}$$

where $M = \begin{bmatrix} 0 & 1 & 0 \\ 0 & 0 & 1 \\ 0 & 0 & 0 \end{bmatrix}$, $N = \begin{bmatrix} 0 \\ b_0 \\ 0 \end{bmatrix}$, $T = \begin{bmatrix} 0 \\ 0 \\ 1 \end{bmatrix}$, $D = \begin{bmatrix} 1 \\ 0 \\ 0 \end{bmatrix}$.

According to (16), LESO is designed as follows:

$$\begin{cases} \dot{z} = M\hat{z} + Nu + \gamma(y - \hat{y}) \\ \hat{y} = Uz \end{cases}, \tag{17}$$

where $z = \begin{bmatrix} z_1 & z_2 & z_3 \end{bmatrix}$ is the state vector of the observer, which is used to observe the state of system $\zeta = [\zeta_1 \ \zeta_2 \ \zeta_3]$; $\gamma = [\gamma_1 \ \gamma_2 \ \gamma_3]^T$ is the observation gain vector of LESO.

The gain value of LESO is obtained from its characteristic equation:

$$\lambda(s) = s^3 + \omega_1 s^2 + \omega_2 s + \omega_3 = (s + \omega_0)^3, \tag{18}$$

where ω_0 is the bandwidth of LESO, denoted as $\omega = [3\omega_0 \ 3\omega_0^2 \ \omega_0^3]^T$.

Remark 1. *The high bandwidth gain of LESO helps to improve the control accuracy of LADRC, but it will cause the output of the controller to increase, and the actuator will consume more energy, which is not conducive to the long-term flight of the quadrotor. This study introduces BP neural network to improve the overall performance of the controller to solve this problem.*

The extended state space observation value of LESO is defined as $\hat{z}_1 = \hat{x}_1$, $\hat{z}_2 = \hat{x}_2$, $\hat{z}_3 = \hat{F}(x, u(n))$. The control law can be written in the following form:

$$u = (u_p - \hat{z}_3)/b_0, \tag{19}$$

where $u_p = k_p(x_d - \hat{z}_1) + k_d(\dot{x}_d - \hat{z}_2) + \ddot{x}_d$ is the output of the PD controller.

4.2. Parameter Tuning Adaptive Law Design

By applying APC to dynamically adjust the k_p and k_d values in the PD controller, the observation error caused by bandwidth selection is compensated. It can not only simplify the controller parameter tuning process, but also improve the control precision of LADRC and the dynamic performance of the system.

Remark 2. *In order to simplify the adjustment of parameter k_p, k_d and avoid errors caused by manual parameter adjustment, we introduce an adaptive law which can adjust k_p, k_d timely. Formulas (36) and (37) provide the adaptive law of k_p, k_d.*

Assumption 1: Assume that a given signal $x_d(t)$ is smooth and bounded such that $\|x_d(t)\| \leq X_d$ is true. Here X_d is a known constant.

Define tracking error:

$$e_1 = x_d - z_1. \tag{20}$$

Derivation can be obtained as follows:

$$\dot{e}_1 = \dot{x}_d - \dot{z}_1 = \dot{x}_d - z_2. \tag{21}$$

Define the filter tracking error:

$$\sigma = \begin{bmatrix} \xi^T & 1 \end{bmatrix} \begin{bmatrix} e_1 \\ \dot{e}_1 \end{bmatrix}, \tag{22}$$

where $\xi^T = a_1$ is a suitable gain vector such that when $\sigma \to 0$, $e_1 \to 0$ is satisfied.

Derivation of σ can be obtained:

$$\dot{\sigma} = \ddot{x}_d - \dot{z}_2 + \begin{bmatrix} 0 & \xi^T \end{bmatrix} \begin{bmatrix} e_1 \\ \dot{e}_1 \end{bmatrix}. \tag{23}$$

From the output of LESO, we can obtain

$$\dot{x}_2 = q(t) + Nu(x) + d(t) = F(x, u(x)). \tag{24}$$

The input of the control is as follows:

$$\delta = -\mu\sigma + u_p - \begin{bmatrix} 0 & \xi^T \end{bmatrix} \begin{bmatrix} e_1 \\ \dot{e}_1 \end{bmatrix}, \tag{25}$$

where μ is any positive number.

In summary, we can obtain

$$\dot{\sigma} = -\mu\sigma + k_p(x_d - \hat{z}_1) + k_d(\dot{x}_d - \hat{z}_2). \tag{26}$$

4.3. BP Neural Network Design

The continuous time-varying wind field disturbance and the continuous reduction of the load mass will cause the control effect of the controller to deteriorate. LESO observes the system status and the total disturbance. However, in the face of continuous time-varying wind field disturbance and changing load quality, the fixed observer bandwidth will lead to larger observation errors and worse control effects. To solve this problem, this

research employs BP neural network (BP) to adjust the bandwidth gain value of LESO online, enhance the observation performance of LESO, and compensate for adverse effects of wind disturbances and changes in load mass.

Remark 3. *LESO can observe each state variable and total disturbance of the quadrotor system according to the input and output of the system. However, due to the discretization of the observer, the bandwidth value of the LESO cannot exceed the sampling period of the system, otherwise it will lead to the divergence of the LESO observations. If the bandwidth value is small, the LESO observation accuracy will be low. Therefore, we introduce APC to compensate the observation error caused by bandwidth selection by dynamically adjusting the k_p and k_d values in the PD controller, so as to improve the control accuracy of LADRC and the dynamic performance of the system. This approach will make LADRC more adaptable and extensive.*

The structure of BP is shown in Figure 3.

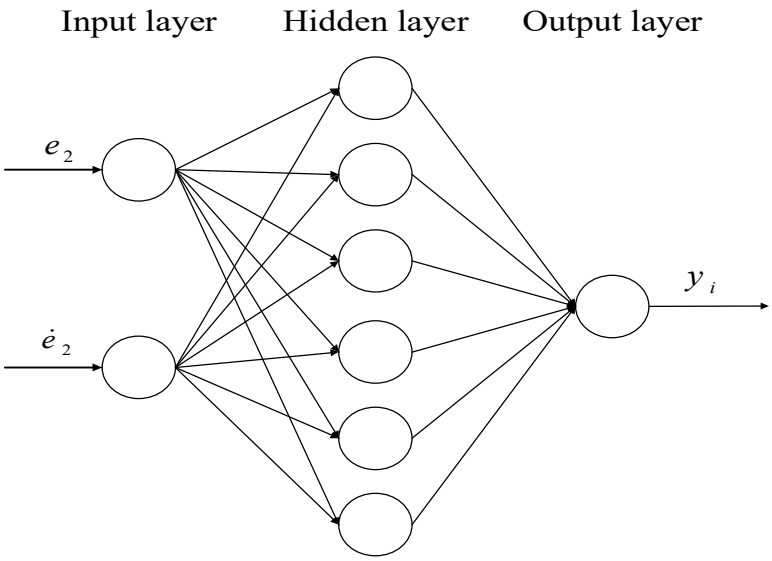

Figure 3. The structure of BP.

The output error is defined as

$$e_2 = x_d - x_1, \tag{27}$$

where x_d is a given signal, x_1 is the state variable of the system; derivation of e_2 can be obtained in the following way:

$$\dot{e}_2 = \dot{x}_d - \dot{x}_1 = \dot{x}_d - x_2. \tag{28}$$

The input of BP neural network can be expressed as

$$IN = \begin{bmatrix} e_2 & \dot{e}_2 \end{bmatrix}^T. \tag{29}$$

The input and output of the hidden layer are

$$\begin{cases} H_a^{in} = \sum\limits_{a=1}^{6} j_a^{in} \cdot IN \\ H_a^{out} = \tan sig\left(H_a^{in}\right) \end{cases} \quad a = 1, 2, 3, 4, 5, 6. \tag{30}$$

The hidden unit is 6, and the excitation function adopts the tangent sigmoid transfer function:

$$\tan sig(k) = \frac{2}{e^{-2k}+1} - 1. \tag{31}$$

Remark 4. *BP neural network adjusts the bandwidth gain vector* $\begin{bmatrix}\beta_1 & \beta_2 & \beta_3\end{bmatrix}$ *of LESO in real time according to the error information of the system. When the system produces output error, the BP neural network will output and adjust* $\begin{bmatrix}\beta_1 & \beta_2 & \beta_3\end{bmatrix}$ *according to the system error information to reduce the observation error of LESO, thereby reducing the system output error and improving the control accuracy of the system.*

The BP neural network that adjusts the LESO bandwidth gain value is divided into three layers of network structure; the input signal of the BP is output error e_2, the differential signal $\dot{e}_2$ of the output error and the bias value k. The number of neurons in the hidden layer is 6 to ensure the strong ability of BP neural network to approximate the error. The output layer contains three neurons, corresponding to the gain vector of LESO. The output of BP neural network can be expressed by the following Formula (34):

$$y(k) = f\left(\sum_{i=1}^{l} \omega_{ik} g\left(\sum_{m=1}^{M} \omega_{mi} v_m\right)\right). \tag{32}$$

Since the BP neural network will normalize the input signal $\begin{bmatrix}e_2 & \dot{e}_2\end{bmatrix}$, its output signal will also be mapped to the range $\begin{pmatrix}-1 & 1\end{pmatrix}$, so the output of the BP cannot be directly used as the bandwidth gain value of LESO. To make the BP−ALADRC controller converge, the output is denormalized to meet the requirement of the gain vector $\begin{bmatrix}\beta_1 & \beta_2 & \beta_3\end{bmatrix}$ of LESO in the BP−ALADRC controller. The gain vector of LESO can be obtained as

$$\beta_k = \beta'_k + f\left(\sum_{i=1}^{l} \omega_{ik} f\left(\sum_{m=1}^{M} \omega_{mi} v_m\right)\right) \cdot k. \tag{33}$$

4.4. Mass Change Adaptive Law Design

The mass of the load carried by the quadrotor may change continuously during the actual working process, which is not conducive to the stability of the system. Therefore, we establish a mass adaptive law based on the height channel to reduce the adverse effects of mass changes on system stability.

According to Formula (12), we can obtain

$$\dot{\chi}_z = U_1 \cos\theta \cos\phi - g - k_f \dot{z}/(M - \Delta m) - \ddot{z}_d + \begin{bmatrix}0 & \xi^T\end{bmatrix}\begin{bmatrix} e_1 \\ \dot{e}_1 \end{bmatrix}. \tag{34}$$

According to the equivalent deterministic principle, we can obtain

$$U_1 = \frac{-\alpha\chi_z - \begin{bmatrix}0 & \xi^T\end{bmatrix}\begin{bmatrix} e_1 \\ \dot{e}_1 \end{bmatrix} + \ddot{z}_d + g + k_f \dot{z}/(M - \Delta\hat{m})}{\cos\phi\cos\theta}, \tag{35}$$

where $\alpha > 0$ is an adjustable parameter. Bringing (37) into (36) can obtain

$$\dot{\chi}_z = \frac{k_f \dot{z}}{M - \Delta\hat{M}} - \alpha\chi_z - \frac{k_f \dot{z}}{M - \Delta M}. \tag{36}$$

Then, $\hat{M}_g = \frac{1}{M - \Delta\hat{m}}$, $M_g = \frac{1}{M - \Delta m}$ are defined, then the estimation error can be expressed as

$$\tilde{M}_g = \hat{M}_g - M_g. \tag{37}$$

Substituting Formula (39) into Formula (38) can obtain

$$\dot{\chi}_z = -\alpha\chi_z + k_f\dot{z}\hat{M}_g - k_f\dot{z}M_g. \tag{38}$$

5. Stability Analysis

To ensure that the system tracking error converges to the zero neighborhood, we design the following adaptive law:

$$\dot{\hat{k}}_p = [\delta k_p(x_d - \hat{z}_1)\varphi]/\widetilde{k}_p, \tag{39}$$

$$\dot{\hat{k}}_d = [\delta k_d(\dot{x}_d - \hat{z}_2)\zeta]/\widetilde{k}_d, \tag{40}$$

$$\dot{\hat{M}}_g = \kappa\dot{\chi}_z k_f\dot{z}. \tag{41}$$

Remark 5. *To avoid $\widetilde{k}_p$ and $\widetilde{k}_d$ being zero, $\dot{\hat{k}}_p$ and $\dot{\hat{k}}_d$ are integrated. The above formula can be rewritten as*

$$\hat{k}_p = \int_0^t [\delta k_p(x_d - \hat{z}_1)\varphi]/\widetilde{k}_p d\tau + k_{p0}, \tag{42}$$

$$\hat{k}_d = \int_0^t [\delta k_d(\dot{x}_d - \hat{z}_2)\zeta]/\widetilde{k}_d d\tau + k_{d0}. \tag{43}$$

Appropriate constants k_{p0} and k_{d0} are chosen to make $\widetilde{k}_p = k_p - \hat{k}_p$ and $\widetilde{k}_d = k_d - \hat{k}_d$ non-zero.

Proof of Theorem 1. A positive definite Lyapunov function is designed as follows.

$$V = \frac{1}{2}\sigma^2 + \frac{1}{2}\chi_z^2 + \frac{1}{2}\widetilde{k}_p\varphi\widetilde{k}_p + \frac{1}{2}\widetilde{k}_d\zeta\widetilde{k}_d + \frac{1}{2}\widetilde{M}_g\kappa\widetilde{M}_g. \tag{44}$$

Taking the derivative of Equation (46),

$$\dot{V} = \sigma\dot{\sigma} + \chi_z\dot{\chi}_z + \widetilde{k}_p\varphi^{-1}\dot{\widetilde{k}}_p + \widetilde{k}_d\zeta^{-1}\dot{\widetilde{k}}_d + \widetilde{M}_g\kappa^{-1}\dot{\widetilde{M}}_g. \tag{45}$$

Bringing (31) and (40) into (47) can obtain

$$\begin{aligned}
\dot{V} &= \sigma\Big[-\mu\sigma + \hat{k}_p(\nu_d - \hat{z}_1) + \hat{k}_d(\dot{\nu}_d - \hat{z}_2)\Big] + \chi_z\Big[-\alpha\chi_z + k_f\dot{z}\hat{M}_g - k_f\dot{z}M_g\Big] \\
&+\widetilde{k}_p\varphi^{-1}\dot{\widetilde{k}}_p + \widetilde{k}_d\zeta^{-1}\dot{\widetilde{k}}_d + \widetilde{M}_g\kappa^{-1}\dot{\widetilde{M}}_g \\
&= -\mu\sigma^2 + \hat{k}_p(\nu_d - \hat{z}_1)\sigma - \alpha\chi_z^2 + k_f\dot{z}\hat{M}_g\chi_z + \hat{k}_d(\dot{\nu}_d - \hat{z}_2)\sigma - k_f\dot{z}M_g\chi_z \\
&+\widetilde{k}_p\varphi^{-1}\dot{\widetilde{k}}_p + \widetilde{k}_d\zeta^{-1}\dot{\widetilde{k}}_d + \widetilde{M}_g\kappa^{-1}\dot{\widetilde{M}}_g \\
&\leq -\mu\sigma^2 + \hat{k}_p(\nu_d - \hat{z}_1)\sigma - \alpha\chi_z^2 + k_f\dot{z}\hat{M}_g\chi_z + \hat{k}_d(\dot{\nu}_d - \hat{z}_2)\sigma - k_f\dot{z}M_g\chi_z \\
&-\widetilde{k}_p\varphi^{-1}\dot{\widetilde{k}}_p + \widetilde{k}_d\zeta^{-1}\dot{\widetilde{k}}_d + \widetilde{M}_g\kappa^{-1}\dot{\widetilde{M}}_g
\end{aligned} \tag{46}$$

Bringing (41), (42) and (43) into (48) can obtain

$$\begin{aligned}
\dot{V} \leq &-\mu\sigma^2 + \hat{k}_p(\nu_d - \hat{z}_1)\sigma - \alpha\chi_z^2 + k_f\dot{z}\hat{M}_g\chi_z + \hat{k}_d(\dot{\nu}_d - \hat{z}_2)\sigma - k_f\dot{z}M_g\chi_z \\
&-\widetilde{k}_p\varphi^{-1}[\delta\hat{k}_p(\nu_d - \hat{z}_1)\varphi]/\widetilde{k}_p + \widetilde{k}_d\zeta^{-1}[\delta k_d(\dot{\nu}_d - \hat{z}_2)\zeta]/\widetilde{k}_d + \widetilde{M}_g\kappa^{-1}\kappa\dot{\chi}_z k_f\dot{z}
\end{aligned} \tag{47}$$

Formula (49) is simplified to obtain

$$\dot{V} \leq -\mu\sigma^2 - \alpha\chi_z^2, \tag{48}$$

where μ and α are positive parameters. Simplifying Equation (49) can obtain

$$\dot{V} \leq 0. \tag{49}$$

Through the above analysis, according to the Lyapunov stability theory, it can be proved that the system is uniformly stable.

According to Barbalat theorem, we can obtain

$$\lim_{t\to\infty}\chi_z(t) = 0, \lim_{t\to\infty}\delta(t) = 0. \tag{50}$$

Therefore, when $t \to \infty$, $\delta(t) \to 0$; this can prove that the quadrotor system is asymptotically stable.

6. Simulation Results and Discussion

The designed controller is tested through numerical simulation in MATLAB. The following three control methods are employed to carry out comparative simulation experiments on the loaded quadrotor. The initial state selected during simulation is $\begin{bmatrix}0 & 0 & 0\end{bmatrix}$rad, $\begin{bmatrix}0 & 0 & 0\end{bmatrix}$m. The quadrotor model parameters are shown in Table 1.

Table 1. Parameters of the quadrotor model.

Symbol	Value
k	0.21 Ns^2/rad^2
M	5 kg
I_x	0.8 $kg \cdot m^2$
I_y	0.8 $kg \cdot m^2$
I_z	1.5 $kg \cdot m^2$
g	9.8 m/s^2
l	0.15 m

Case Study 1. Quadrotor mass M = 5 kg, load mass m = 3 kg; given input signal: Z_d = 6 m, θ_d = 35 °, ϕ_d = 45 °, ψ_d = 55 °. The simulation results of BP−ALADRC are compared with LADRC and DSADRC. Figure 4 is the output curves, and Figure 5 is the output curves and error curves. In the altitude channel, BP−ALADRC has the fastest tracking speed, BP−ALADRC and DSADRC can reach stability within 1 s and 1.2 s, respectively, while LADRC needs 2.3 s to achieve stable tracking. In the channels of pitch and row angle, while maintaining fast track speed, BP−ALADRC has significantly less overshoot than DSADRC and LADRC. In the yaw angle channel, BP−ALADRC was significantly faster to respond. In summary, the BP−ALADRC controller has the fastest tracking speed and smallest overshoot compared to DSADRC and LADRC, and can quickly and stably reach system stabilization, which proves the effectiveness of the BP−ALADRC controller.

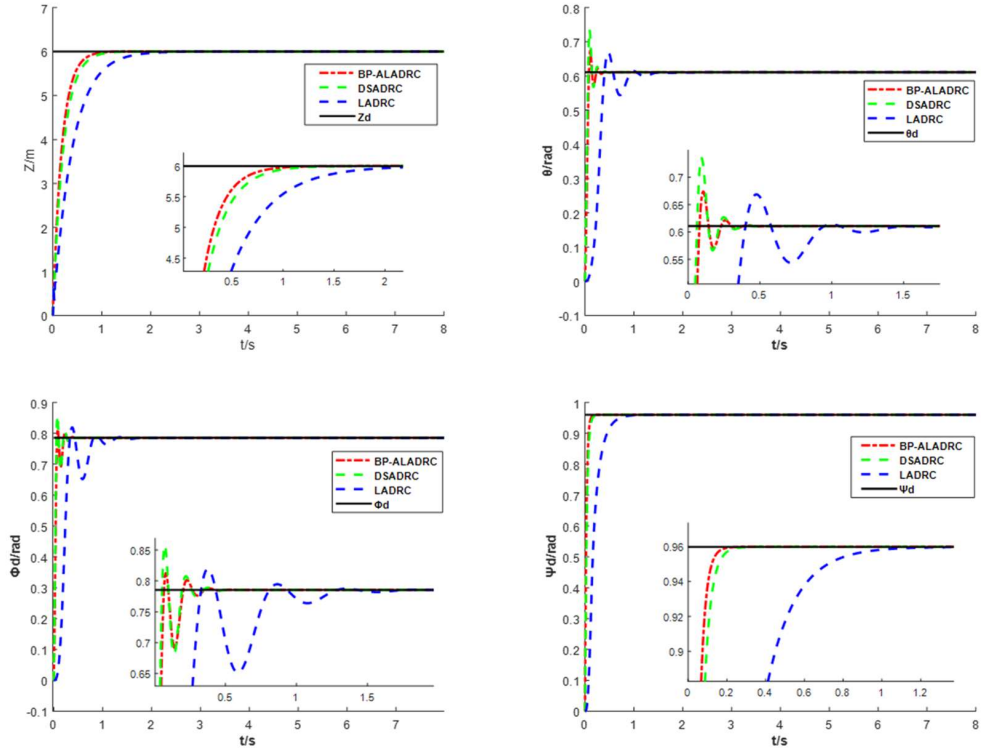

(**a**) (**b**)

Figure 4. System output: (**a**) Altitude and Roll angle output; (**b**) Pitch and Yaw angle output.

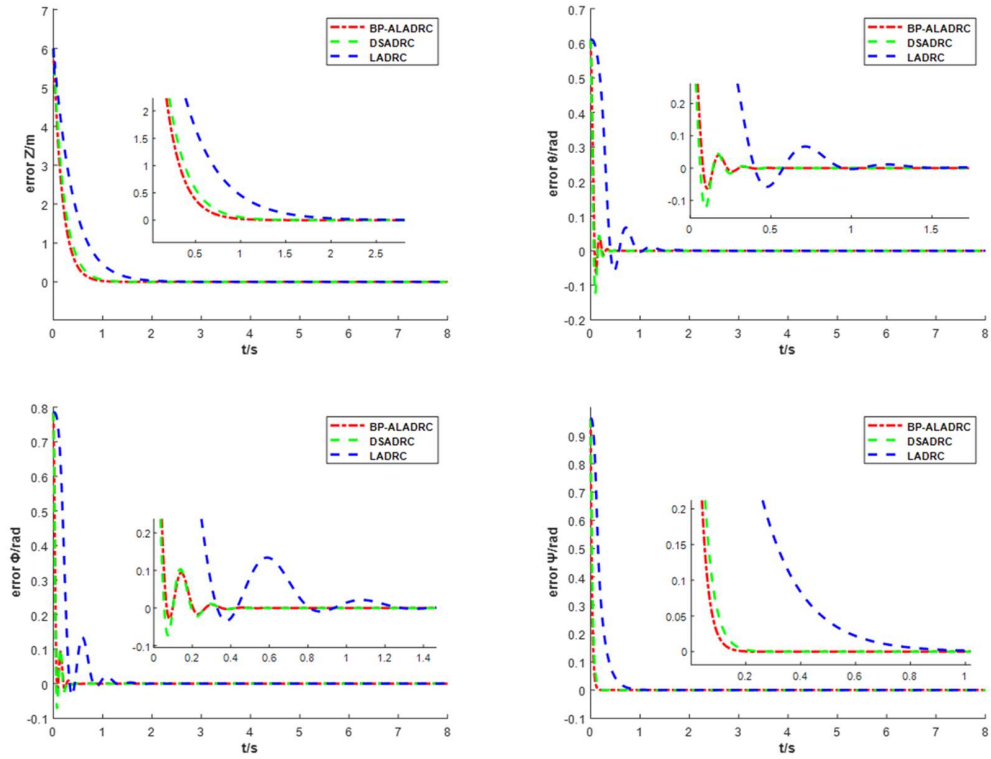

(**a**) (**b**)

Figure 5. System output errors: (**a**) Altitude and Roll angle output errors; (**b**) Pitch and Yaw angle output errors.

Case Study 2. In this test, we use BP−LADRC without PD adaptive law as a comparison. To simulate the external interference received by the quadrotor during the working process, we use Gaussian white noise with a variance of 2.5 and a mean value of 0 to represent the external interference. As shown in Figure 6.

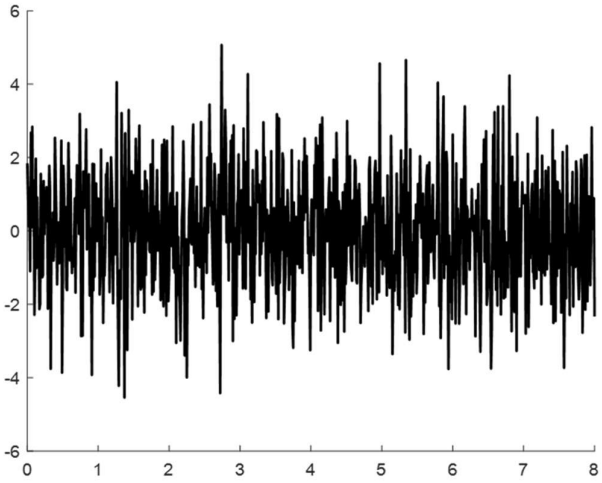

Figure 6. Gaussian noise simulation diagram.

According to Figures 7 and 8, when the quadrotor is disturbed, the tracking curve fluctuation of BP−ALADRC to the reference input is the smallest; BP−ALADRC has the fastest tracking speed, while LADRC has the slowest tracking speed; the overshoot of BP−ALADRC is significantly smaller than that of BP−LADRC without PD adaptive law; to sum up, the introduction of BP can reduce the overshoot and speed up the system response speed. At the same time, the addition of the PD adaptive law further increases the stability of the system, eliminates the adverse effects of parameter deviations on the system, further reduces the system overshoot. Meanwhile, system response speed is further accelerated in the height channel, and the control effect of the controller is improved.

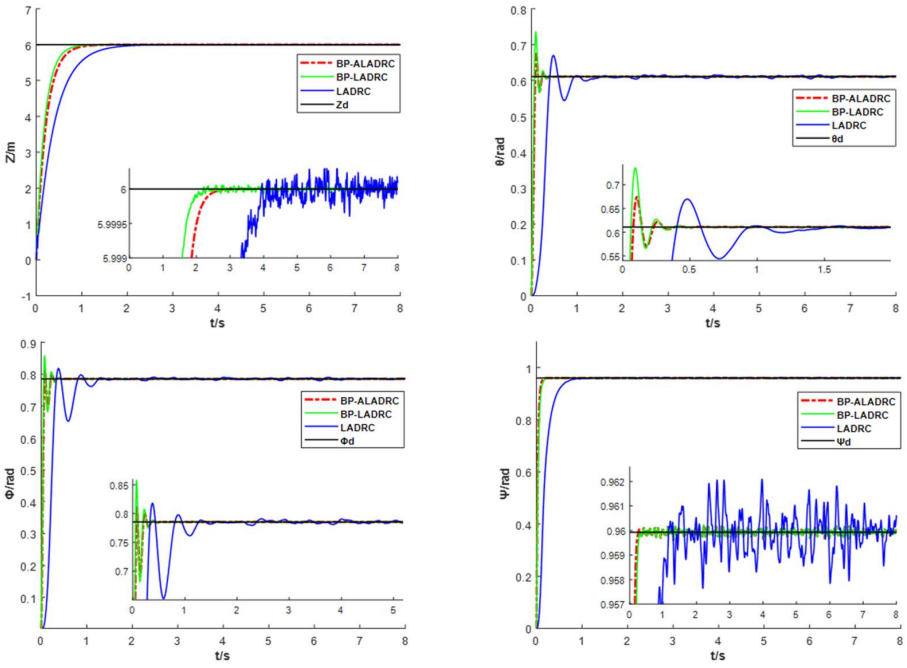

(**a**) (**b**)

Figure 7. System output: (**a**) Altitude and Roll angle output; (**b**) Pitch and Yaw angle output.

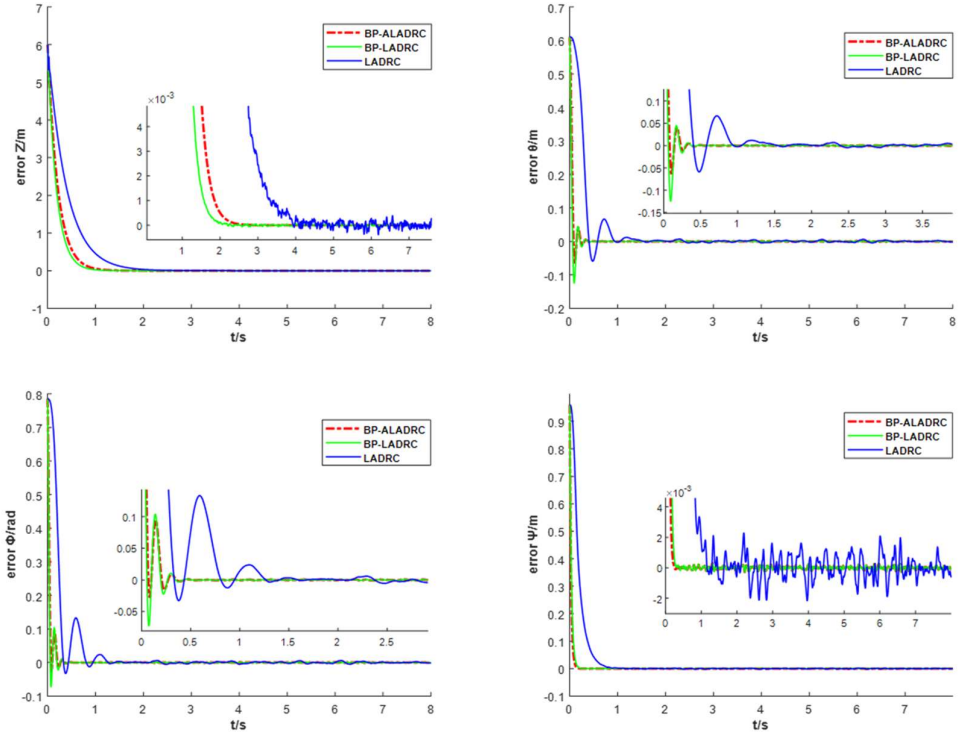

Figure 8. System output errors: (**a**) Altitude and Roll angle output errors; (**b**) Pitch and Yaw angle output errors.

From Figure 9, when the quadrotor is affected by external disturbances, the parameters k_p and k_d of the PD controller will be adjusted timely on the basis of the system state, which can eliminate the parameter deviation.

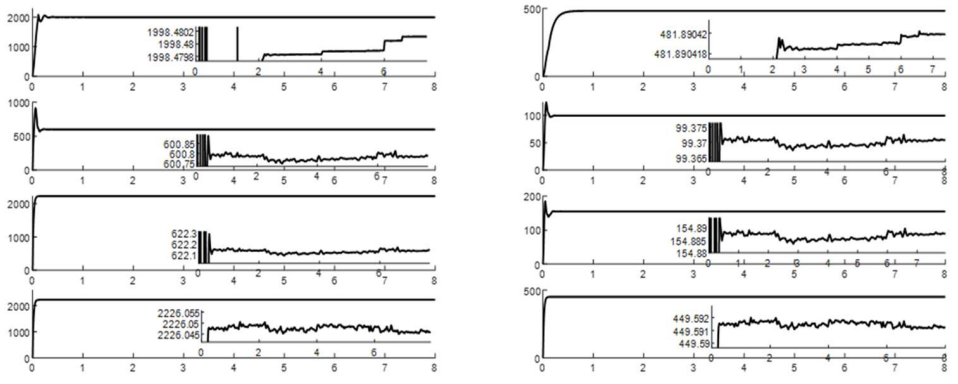

Figure 9. k_p and k_d adaptive values: (**a**) k_p adaptive value; (**b**) k_d adaptive value.

Case Study 3. The load mass carried by the quadrotor will change in real time; in this test, we make the load mass decrease continuously, and the system input signal remains unchanged. The BP−ALADRC controller is compared with mass adaptive control law and the BP−ALADRC controller without mass adaptive control law. Figure 10 is a load mass change diagram.

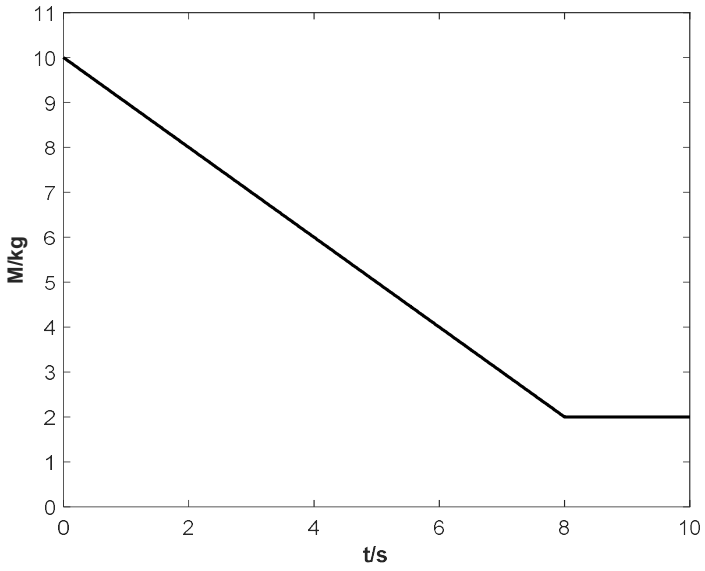

Figure 10. Load mass variation diagram.

Figures 11 and 12 show that the BP−ALADRC with the mass adaptive law can effectively reduce the error caused by the load mass change, and the BP−ALADRC without the mass adaptive law has significantly larger overshoots in the pitch angle and roll angle channels. At the same time, the response speed of the system is not as good as that of the BP−ALADRC controller with the quality adaptive law.

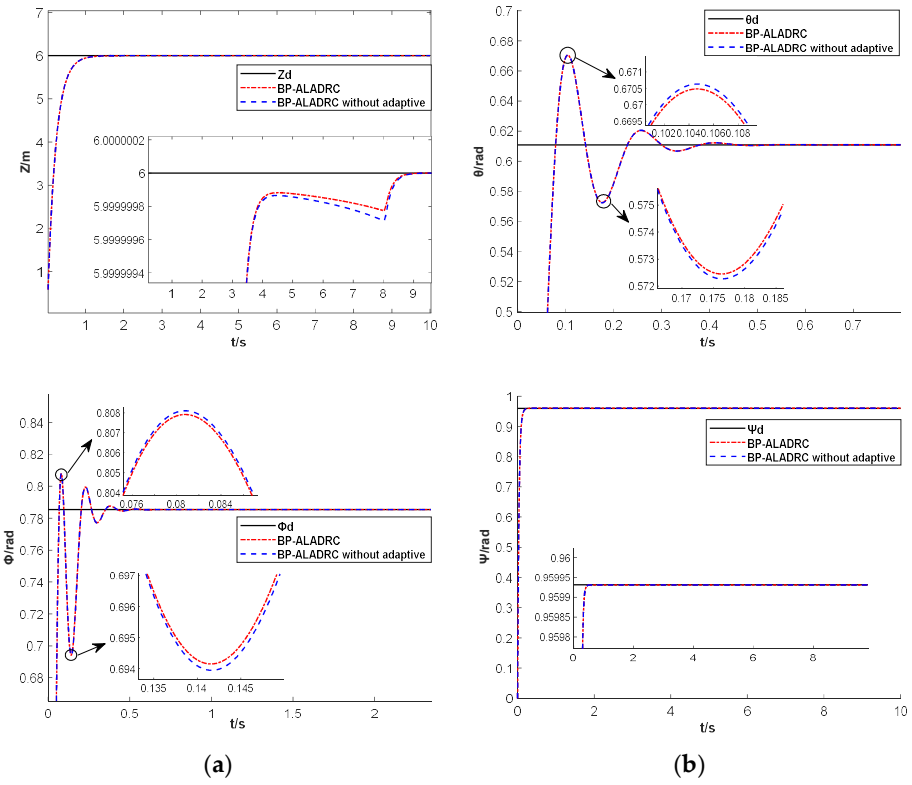

(**a**) (**b**)

Figure 11. System output: (**a**) Altitude and Roll angle output; (**b**) Pitch and Yaw angle output.

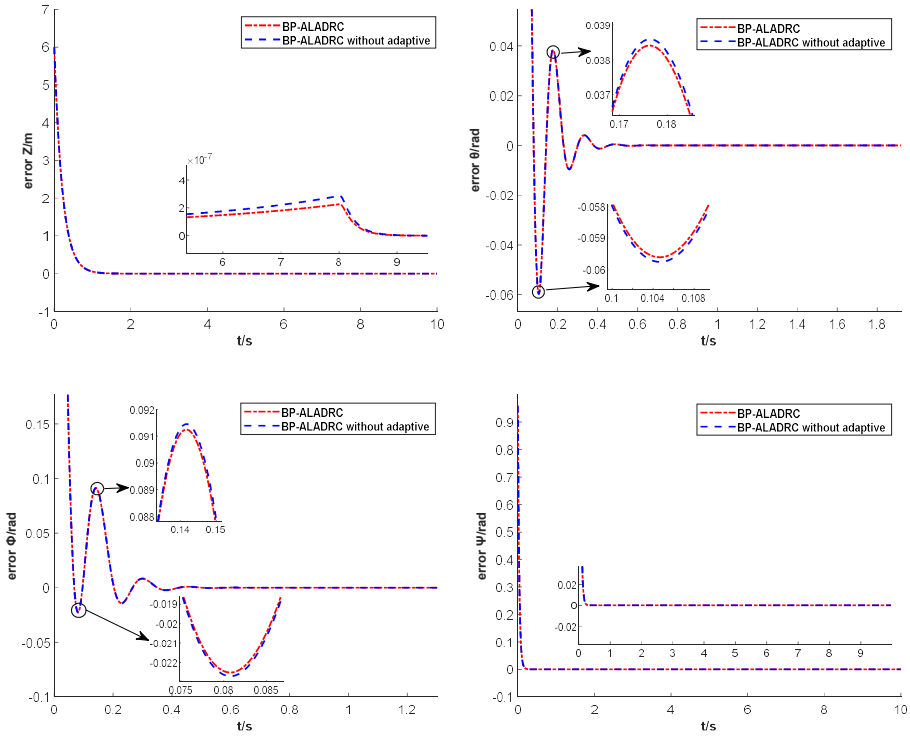

Figure 12. System output errors: (**a**) Altitude and Roll angle output errors; (**b**) Pitch and Yaw angle output errors.

In Case Study 1, the control scheme designed in this paper and the control methods of LADRC [30] and DSADRC are applied to the attitude control of the quadrotor system. It can be seen that the controller designed in this paper has less overshoot and faster response speed in the dynamic response process. In Case Study 2, we conducted interference experiments. By adding white noise interference to the system, we verified that the controller has a strong ability to suppress interference. Finally, Case Study 3 shows that the controller has strong adaptability to the change of load mass. All the above case studies show that the designed controller can track the given signal quickly and stably, effectively reducing the adverse effects of interference on the quadrotor system. It is proved that the controller designed in this paper has more significant signal tracking ability, interference suppression ability and better system adjustment ability. In addition, the introduction of adaptive control effectively compensates the observation error of LESO, making the controller more robust. Finally, when the load mass of the quadrotor changes, the designed mass adaptive law can effectively overcome the adverse effects of mass changes on the system and enhance the stability of the system.

7. Conclusions

In order to improve the attitude control performance of the quadrotor, this paper considers the change of the load mass of the quadrotor, establishes a dynamic model of the quadrotor with variable mass, and designs a composite control scheme based on LADRC. For the problems of many parameters of LADRC controller, difficult adjustment and large error of manual parameter adjustment, this paper proposes BP neural network and adaptive control to optimize and adjust LADRC parameters. The BP neural network is used to dynamically optimize and adjust the bandwidth value of LESO in real time, which improves the disturbance observation accuracy of the system. At the same time, the introduction of adaptive control reduces the observation error of LESO and the parameter deviation of PD controller. These ensure the stability of the quadrotor system in the complex and changeable working environment. Finally, all the case studies show that for

the same given attitude angle and altitude, the designed control system has the advantages of small overshoot, fast system response and strong robustness compared with LADRC and DSADRC controllers. In addition, the designed mass adaptive law can also effectively reduce the adverse effects of load mass changes on the system and further enhance the stability of the system. At present, due to the limitations of experimental conditions, this paper only carried out theoretical research. In the future work, we will verify the effectiveness of the control scheme in practical applications.

Author Contributions: Y.G.: contributed to the conception of the study, performed the experiment, performed the data analyses and wrote the manuscript; G.Z.: contributed to the conception of the study; T.Z.: helped perform the analysis with constructive discussions. All authors have read and agreed to the published version of the manuscript.

Funding: This research received no external funding.

Institutional Review Board Statement: Not applicable.

Informed Consent Statement: Not applicable.

Data Availability Statement: Not applicable.

Conflicts of Interest: The authors declare no conflict of interest.

References

1. Comba, L.; Biglia, A.; Aimonino, D.R.; Gay, P. Unsupervised detection of vineyards by 3D point-cloud UAV photogramme-try for precision agriculture. *Comput. Electron. Agric.* **2018**, *155*, 84–95. [CrossRef]
2. Tokekar, P.; Vander Hook, J.; Mulla, D.; Isler, V. Sensor planning for a symbiotic UAV and UGV system for precision agriculture. *IEEE Trans. Robot.* **2016**, *32*, 1498–1511. [CrossRef]
3. Roberge, V.; Tarbouchi, M.; Labonté, G. Fast Genetic Algorithm Path Planner for Fixed-Wing Military UAV Using GPU. *IEEE Trans. Aerosp. Electron. Syst.* **2018**, *54*, 2105–2117. [CrossRef]
4. Shakeel, T.; Arshad, J.; Jaffery, M.H.; Rehman, A.U.; Eldin, E.T.; Ghamry, N.A.; Shafiq, M. A Comparative Study of Control Methods for X3D Quadrotor Feedback Trajectory Control. *Appl. Sci.* **2022**, *12*, 9254. [CrossRef]
5. Islam, M.; Okasha, M.; Sulaeman, E. A model predictive control (mpc) approach on unit quaternion orientation based quadrotor for trajectory tracking. *Int. J. Control. Autom. Syst.* **2019**, *17*, 2819–2832. [CrossRef]
6. Eskandarpour, A.; Sharf, I. A constrained error-based MPC for path following of quadrotor with stability analysis. *Nonlinear Dyn.* **2020**, *99*, 899–918. [CrossRef]
7. Falcon, R.; Rios, H.; Dzul, A. Comparative analysis of continuous sliding-modes control strategies for quad-rotor robust tracking. *Control. Eng. Pract.* **2019**, *90*, 241–256. [CrossRef]
8. Okyere, E.; Bousbaine, A.; Poyi, G.T.; Joseph, A.K.; Andrade, J.M. Lqr controller design for quad-rotor helicopters. *J. Eng.* **2019**, *17*, 4003–4007. [CrossRef]
9. Jian, P.; Changlong, L. UAV attitude control with LQR controller based on extended state observer. *Syst. Simul.* **2018**, *30*, 753–759.
10. Rodríguez-Guerrero, L.; Benítez-Morales, A.; Santos-Sánchez, O.-J.; García-Pérez, O.; Romero-Trejo, H.; Ordaz-Oliver, M.-O.; Ordaz-Oliver, J.-P. Robust Backstepping Control Applied to UAVs for Pest Recognition in Maize Crops. *Appl. Sci.* **2022**, *12*, 9075.
11. Nigro, M.; Pierri, F.; Caccavale, F. Control of an Omnidirectional UAV for Transportation and Manipulation Tasks. *Appl. Sci.* **2021**, *11*, 10991. [CrossRef]
12. Fan, Y.; Guo, H.; Han, X.; Chen, X. Research and Verification of Trajectory Tracking Control of a Quadrotor Carrying a Load. *Appl. Sci.* **2022**, *12*, 1036. [CrossRef]
13. Chen, X.; Zhao, Y.; Fan, Y. Adaptive Integral Backstepping Control for a Quadrotor with Suspended Flight. In Proceedings of the 2020 5th International Conference on Automation. Control and Robotics Engineering (CACRE), Dalian, China, 19–20 September 2020; pp. 226–234.
14. Han, J.Q. From PID to Active Disturbance Rejection Control. *IEEE Trans. Ind. Electron.* **2009**, *56*, 900–906. [CrossRef]
15. Zhang, Q.; Wei, Y.; Li, X. Quadrotor Attitude Control by Fractional-Order Fuzzy Particle Swarm Optimization-Based Active Disturbance Rejection Control. *Appl. Sci.* **2021**, *11*, 11583. [CrossRef]
16. Yuan, C.; Zhou, X.; Ma, Y. DC Bus Voltage Control of Wind Power Inverter Based on First-Order LADRC. *IEEE Access* **2021**, *10*, 3263–3274. [CrossRef]
17. Zhao, F.; Wang, X.; Zhu, T. Low-Frequency Passivity-Based Analysis and Damping of Power-Synchronization Controlled Grid-Forming Inverter. *IEEE J. Emerg. Sel. Top. Power Electron.* **2022**. [CrossRef]
18. Hua, L.; Zhang, J.; Li, D.; Xi, X. Fault-Tolerant Active Disturbance Rejection Control of Plant Protection of Unmanned Aerial Vehicles Based on a Spatio-Temporal RBF Neural Network. *Appl. Sci.* **2021**, *11*, 4084. [CrossRef]
19. Guo, B.; Bacha, S.; Alamir, M.; Mohamed, A.; Boudinet, C. LADRC applied to variable speed micro-hydro plants: Experimental validation. *Control. Eng. Pract.* **2019**, *85*, 290–298. [CrossRef]

20. Zhou, Y.; Luo, D.; Wu, B.; Cheng, B.; Lin, Q. Active vibration isolation system based on the LADRC algorithm for atom interferometry. *Appl. Opt.* **2020**, *59*, 3487–3493. [CrossRef]
21. Geng, X.; Zhu, Q.; Liu, T.; Na, J. U-model based predictive control for nonlinear processes with input delay. *J. Process Control.* **2019**, *75*, 156–170. [CrossRef]
22. Wang, H.; Huang, H. Property and applications of extended state observer. *Control. Decis.* **2013**, *28*, 1078–1082.
23. Zhang, Y.; Chen, Z.; Sun, M. Trajectory tracking control for a quadrotor unmanned aerial vehicle based on dynamic surface active disturbance rejection control. *Trans. Inst. Meas. Control.* **2020**, *42*, 2198–2205. [CrossRef]
24. Wu, J.; Peng, H.; Chen, Q.; Penge, X. Modeling and control approach to a distinctive quadrotor helicopter. *ISA Trans.* **2014**, *53*, 173–185. [CrossRef] [PubMed]
25. Cai, Z.; Lou, J.; Zhao, J.; Wu, K.; Liu, N.; Wang, Y.X. Quadrotor trajectory tracking and obstacle avoidance by chaotic grey wolf optimization-based active disturbance rejection control. *Mech. Syst. Signal Process.* **2019**, *128*, 636–654. [CrossRef]
26. Zhao, Z.; Cao, D.; Yang, J.; Wang, H. High-order sliding mode observer-based trajectory tracking control for a quadrotor UAV with uncertain dynamics. *Nonlinear Dyn.* **2020**, *102*, 2583–2596. [CrossRef]
27. Tang, P.; Lin, D.; Zheng, D.; Fan, S.; Ye, J. Observer based finite-time fault tolerant quadrotor attitude control with actuator faults. *Aerosp. Sci. Technol.* **2020**, *104*, 105968. [CrossRef]
28. Nekoukar, V.; Dehkordi, N.M. Robust path tracking of a quadrotor using adaptive fuzzy terminal sliding mode control. *Control. Eng. Pract.* **2021**, *110*, 104763. [CrossRef]
29. Wang, B.; Yu, X.; Mu, L.; Zhang, Y. Disturbance observer-based adaptive fault-tolerant control for a quadrotor helicopter subject to parametric uncertainties and external disturbances. *Mech. Syst. Signal Process.* **2019**, *120*, 727–743. [CrossRef]
30. Liang, X.; Li, J.; Zhao, F. Attitude Control of Quadrotor UAV Based on LADRC Method. In Proceedings of the 2019 Chinese Control and Decision Conference (CCDC), Nanchang, China, 3–5 June 2019; pp. 1924–1929.